



Open camera or QR reader and scan code to access this article and other resources online.

Recapitulation of Skewed X-Inactivation in Female Ornithine Transcarbamylase-Deficient Primary Human Hepatocytes in the FRG Mouse: A Novel System for Developing Epigenetic Therapies

Sharon C. Cunningham,¹ Eva B. van Dijk,¹ Erhua Zhu,¹ Maya Sugden,¹ Mawj Mandwie,¹ Susan Siew,^{2,3} Beena Devanapalli,⁴ Adviyee Ayper Tolun,^{3,4} Anne Klein,⁵ Laurence Wilson,^{5,6} Nader Aryamanesh,⁷ Paul Gissen,⁸ Julien Baruteau,⁸ Kaustuv Bhattacharya,^{3,9} and Ian E. Alexander^{1,3,*}

¹Gene Therapy Research Unit, Faculty of Medicine and Health, Children's Medical Research Institute, The University of Sydney and Sydney Children's Hospitals Network, Westmead, Australia.

²Department of Gastroenterology, James Fairfax Institute of Paediatric Nutrition, Sydney Children's Hospitals Network, Westmead, Australia.

³Discipline of Child and Adolescent Health, Faculty of Medicine and Health, The University of Sydney, Westmead, Australia.

⁴NSW Biochemical Genetics Service, The Children's Hospital at Westmead, Westmead, Australia.

⁵Australian e-Health Research Centre, Commonwealth Scientific and Industrial Research Organisation (CSIRO), Sydney, Australia.

⁶Department of Biomedical Sciences, Macquarie University, Macquarie Park, Australia.

⁷Embryology Research Unit, Bioinformatics Group, Children's Medical Research Institute, University of Sydney, Westmead, Australia.

⁸National Institute for Health Research Great Ormond Street Hospital Biomedical Research Centre, University College London, London, United Kingdom.

⁹Genetic Metabolic Disorders Service, The Children's Hospital at Westmead, Sydney, Australia.

Realization of the immense therapeutic potential of epigenetic editing requires development of clinically predictive model systems that faithfully recapitulate relevant aspects of the target disease pathophysiology. In female patients with ornithine transcarbamylase (OTC) deficiency, an X-linked condition, skewed inactivation of the X chromosome carrying the wild-type OTC allele is associated with increased disease severity. The majority of affected female patients can be managed medically, but a proportion require liver transplantation. With rapid development of epigenetic editing technology, reactivation of silenced wild-type OTC alleles is becoming an increasingly plausible therapeutic approach. Toward this end, privileged access to explanted diseased livers from two affected female infants provided the opportunity to explore whether engraftment and expansion of dissociated patient-derived hepatocytes in the FRG mouse might produce a relevant model for evaluation of epigenetic interventions. Hepatocytes from both infants were successfully used to generate chimeric mouse–human livers, in which clusters of primary human hepatocytes were either OTC positive or negative by immunohistochemistry (IHC), consistent with clonal expansion from individual hepatocytes in which the mutant or wild-type OTC allele was inactivated, respectively. Enumeration of the proportion of OTC-positive or -negative human hepatocyte clusters was consistent with dramatic skewing in one infant and minimal to modest skewing in the other. Importantly, IHC and fluorescence-activated cell sorting analysis of intact and dissociated liver samples from both infants showed qualitatively similar patterns, confirming that the chimeric mouse–human liver model recapitulated the native state in each infant. Also of importance was the induction of a treatable metabolic phenotype, orotic aciduria, in mice, which correlated with the presence of clonally expanded OTC-negative primary human hepatocytes. We are currently using this unique model to explore CRISPR-dCas9-based epigenetic targeting strategies in combination with efficient adeno-associated virus (AAV) gene delivery to reactivate the silenced functional OTC gene on the inactive X chromosome.

Keywords: liver, X-inactivation, ornithine transcarbamylase deficiency, xenograft mouse, epigenetics, adeno-associated viral vector

*Correspondence: Prof. Ian E. Alexander, Gene Therapy Research Unit, Faculty of Medicine and Health, Children's Medical Research Institute, The University of Sydney and Sydney Children's Hospitals Network, Westmead 2145, Australia. E-mail: ian.alexander@health.nsw.gov.au

INTRODUCTION

CONVENTIONAL GENE THERAPY strategies have commonly involved gene addition, but more recently, there has been a growing focus on gene editing approaches. These are generally best suited to autosomal recessive disorders and a proportion of X-linked disorders in males, in which only mutant alleles are present. However, in heterozygous females carrying X-linked conditions, a healthy allele is present in every cell, but is frequently transcriptionally silenced.

This is the consequence of X-inactivation, whereby one X chromosome in each cell is inactivated by epigenetic mechanisms during early development.¹ The X chromosome contains close to 1,000 genes, with at least half implicated in X-linked disease.² While most published reports exploring the development of epigenetic therapies have focused on neurological disorders,^{3–5} liver-based X-linked diseases such as ornithine transcarbamylase (OTC) deficiency (OMIM no. 311250) are also potentially curable by therapeutic modulation of the epigenome.

OTC is a key enzyme of the urea cycle, which removes ammonia from the body, a highly neurotoxic metabolite produced by the breakdown of proteins and other nitrogen-containing molecules. Deficiency of OTC is associated with recurrent life-threatening hyperammonemic decompensation and adverse neurological development. While males are most severely affected, females exhibit a wide phenotypic spectrum from severe life-threatening symptoms during the neonatal period to asymptomatic or milder late-onset forms.

An estimated 20–30% of OTC carrier females develop symptoms in early childhood,⁶ requiring chronic medical therapies, with transplantation as the only curative option. A major driver of this phenotypic variability is random skewing of X chromosome inactivation, with disease severity correlating with increased skewing in favor of inactivation of the X chromosome carrying the wild-type OTC allele. Reactivation of this healthy allele on the inactivated X chromosome through epigenetic interventions offers an intrinsic cure.

A major limitation in the development of such approaches, however, is the availability of clinically predictive models that faithfully recapitulate relevant aspects of disease pathophysiology. This is particularly challenging in complex disease phenotypes involving both genetic and epigenetic mechanisms. We have pioneered the use of chimeric mouse–human livers in the humanized FRG (hFRG) mouse model⁷ to develop novel vector delivery systems based on recombinant adeno-associated virus (rAAV) with unprecedented levels of human hepatocyte tropism.⁸

This capability, combined with privileged access to liver explants from pediatric patients undergoing liver

transplantation, has allowed us to explore the configuration of disease-specific models in the FRG mouse. Notably, liver explants have been acquired from two female infants with clinically troubling OTC deficiency, thereby providing a unique opportunity to investigate epigenetic-based therapeutic approaches in this disease context.

This study explores skewing of X-inactivation in both native patient liver explants and dissociated patient-derived hepatocytes following engraftment and expansion in the FRG mouse liver. Immunohistochemical and molecular analyses revealed that the levels of skewing present in intact liver tissue were recapitulated in chimeric mouse–human livers. Moreover, the dissociated hepatocytes induced a treatable biochemical phenotype in the FRG mouse once OTC-negative clusters of patient-derived hepatocytes were expanded to a critical threshold.

These results support the use of this unique model system to assess epigenome editing strategies *in vivo* using highly efficient AAV-mediated gene delivery.

MATERIALS AND METHODS

Acquisition and sampling of patient liver

Liver explants were obtained from pediatric patients with OTC deficiency undergoing transplantation at The Children's Hospital at Westmead, Westmead, NSW, Australia, with informed parental consent and approval by the Sydney Children's Hospitals Network Human Ethics Committee (HREC/18/SCHN/236). Liver was sampled for histological and molecular analyses, and hepatocytes were isolated from remaining tissue by a two-step collagenase perfusion procedure⁹ and cryopreserved.

Mutation analysis data were obtained from the Molecular Genetics Laboratory within The Children's Hospital at Westmead.

Establishment of chimeric mouse–human liver in the FRG mouse model

All animal care and experimental procedures were evaluated and approved by the Animal Ethics Committee of the Children's Medical Research Institute and The Children's Hospital at Westmead. FRG mice (immune-deficient Fah knockouts),⁷ breeding pairs, were obtained from Professor Markus Grompe (Oregon Health and Science University, Portland, OR). Mice were housed in individually ventilated cages with free access to drinking water supplemented with 2-(2-nitro-4-trifluoromethylbenzoyl)-1,3-cyclohexanedione (NTBC; 8 μ g/mL) before engraftment.

Dissociated human hepatocytes isolated from donor explant livers were engrafted into female mice (6–8 weeks old) through splenic injection⁷ (1×10^6 cells per mouse). Mice were cycled on and off NTBC to promote selective repopulation of the liver with patient-derived primary human hepatocytes. Engraftment levels were estimated by

measuring human serum albumin by enzyme-linked immunosorbent assay (Bethyl Laboratories, Inc., Montgomery, TX).

OTC enzymatic activity

OTC activity was determined *in situ* in fixed frozen liver sections and liver lysates, as previously described.¹⁰ The lysate assay was modified to enable a 96-well plate format by scaling reaction volumes down to a final 200 μ L containing 50–100 mg of liver tissue. Wild-type liver (21-year-old male) was used as a positive control and to estimate residual OTC activity in patient-derived samples.

Sections were cover-slipped using EpreDia™ Imm-mount™ (Fisher Scientific; Cat no. 9990402) and imaged with the Zeiss Axio Imager M1 microscope equipped with an MRm monochrome camera and Zeiss Zen Blue software. Image analysis to quantify OTC-positive areas, as an estimate of percentage positive cells, was done using FIJI/ImageJ software.¹¹

Immunohistochemistry

Liver samples were fixed in either (1) 4% (w/v) paraformaldehyde (PFA) in phosphate-buffered saline (PBS) at 4°C overnight, followed by cryoprotection through 10%, 20%, and 30% (w/v) sucrose in PBS, and frozen in optimal cutting temperature O.C.T. compound (Tissue-Tek; Sakura Finetek USA, Torrance, CA); or (2) 10% (v/v) buffered formalin at room temperature (RT) for 48–72 h, transferred to 70% (v/v) ethanol, and paraffin embedded. Embedding and sectioning were carried out at Westmead Histology (Westmead Research Hub).

Analyses on patient liver were performed on PFA-fixed tissue. Sections (5 μ m) were permeabilized in methanol, blocked in PBS/fetal bovine serum/donkey serum, and incubated with anti-OTC antibody (rabbit polyclonal; Sigma-Aldrich; Cat no. HPA000243; 1:100 dilution) overnight at 4°C. After washing in PBS/0.05% (v/v) Tween-20, sections were incubated with donkey anti-rabbit Alexa Fluor 594 (Invitrogen™; Cat no. A21207; 1:500 dilution) for 1 h at RT.

Sections were then incubated with rabbit anti-human glyceraldehyde 3-phosphate dehydrogenase (GAPDH) Alexa Fluor 647 (Abcam; Cat no. ab215227; 1:800 dilution) for 1 h at RT. 4',6-Diamidino-2-phenylindole (DAPI) was used to identify nuclei and included in the final wash steps (PBS/0.1% (v/v) Tween-20, PBS alone, PBS/DAPI, and PBS alone). Sections were cover-slipped using Imm-mount and imaged with the Zeiss Axio Imager Z2 equipped with an AxioCam 506 monochrome camera and Zen software.

Analyses on chimeric mouse–human liver were performed on formalin-fixed paraffin-embedded tissue. Paraffin sections (4 μ m) were dewaxed and hydrated, then antigen retrieval was performed in a Tris-ethylenediaminetetraacetic acid (EDTA) buffer (10 mM Tris base, 1 mM EDTA solu-

tion, and 0.05% (v/v) Tween-20, pH 9.0) in a Pelco BioWave 34700-230 microwave set at 98°C for 15 min. After blocking, immunostaining was carried out, as described above. Image analysis to quantify OTC-positive areas, as an estimate of percentage positive cells and to measure cluster size, was done using FIJI/ImageJ software.¹¹

Quantitation of OTC in dissociated hepatocytes

The proportion of OTC-positive and -negative human hepatocytes was determined by fluorescence-activated cell sorting (FACS) in cryopreserved patient hepatocytes and in hepatocytes from hFRG dissociated as previously described.¹² Cells were labeled with LIVE/DEAD™ Fixable Near-IR (Invitrogen; Cat no. L10119), fixed in 4% (w/v) PFA in PBS for 15 min, and permeabilized with precooled methanol for 10 min.

The cells were then incubated with rabbit anti-OTC antibody (Sigma; no. HPA000243; 1:100 dilution) for 90 min at RT. After washing, the cells were incubated with donkey anti-rabbit AF647 (Invitrogen; Cat no. A-31573; 1:400 dilution) for 40 min at RT, washed again, and then resuspended in PBS for processing on the BD LSRFortessa Cell Analyzer and analysis using FlowJo software.

Human OTC allele-specific mRNA expression analysis

Total RNA was extracted from ~50 mg of dissociated human hepatocytes using TRIzol (Invitrogen, Thermo Fisher Scientific) and treated with DNase I (Invitrogen, Thermo Fisher Scientific). Reverse transcription using the SuperScript III First-Strand Synthesis SuperMix Kit (Invitrogen, Thermo Fisher Scientific) generated a cDNA template for polymerase chain reaction (PCR) amplification using human sequence-specific primers (Supplementary Table S1) flanking disease mutations.

PCR products were analyzed by Sanger sequencing.

AAV vector production

The human OTC coding sequence (codon-optimized) under the transcriptional control of a hepatocyte-specific promoter was inserted into an AAV vector. As a control, the OTC coding sequence was replaced with enhanced green fluorescent protein. Vectors were pseudo-serotyped with the human liver tropic LK03 capsid⁸ produced in human embryonic kidney 293 cells by triple plasmid transfection. Titer was assigned by real-time quantitative PCR using primers and probe (Supplementary Table S1) targeting the bovine growth hormone polyadenylation signal sequence in the vector.

Urinary orotate analysis in FRG mice

Urine was collected by placing mice on a wire mesh over Whatman filter paper for 24 h. Circular punches (3 mm diameter) were sampled from urine spots (10 per paper) and urine eluted in 300 μ L of water. Orotate and

creatinine were measured using liquid chromatography/tandem mass spectrometry on a Waters XEVO TQ-S spectrometer (Waters Australia, Rydalmere, Australia). To measure orotate, 50 μL of each sample was transferred to a 96-well, polypropylene v-base plate (Nunc, Roskilde, Denmark).

An internal standard (100 $\mu\text{mol}/1,3\text{-}^{15}\text{N}_2$ orotic acid; Cambridge Isotope Laboratories, Andover, MA) was added to each sample (50 $\mu\text{L}/\text{well}$). Orotate was analyzed in negative ion mode by multiple reaction monitoring using transitions 155.1 > 111.1 and 157.1 > 113.1 for native and stable isotope-labeled orotic acid, respectively. Results were standardized against creatinine: 5 μL of each sample was transferred to a 96-well, polypropylene v-base plate and diluted with 100 μL of water.

An internal standard (88 $\mu\text{mol}/\text{L}$ creatinine- d_3 ; Cambridge Isotope laboratories, Andover, MA) was added to each sample (5 $\mu\text{L}/\text{well}$). Creatinine was analyzed in positive ion mode by multiple reaction monitoring using transitions 114.15 > 86.19 and 117.15 > 89.19 for native and stable isotope-labeled creatinine, respectively.

Statistics

The nonparametric Mann–Whitney *U* test was applied to all data sets where normal distribution was not assumed due to small sample size. For measurement of elevation of urinary orotate, two-way repeated-measures analysis of variance (ANOVA) was performed. GraphPad Prism (version 9.4.1; GraphPad Software, La Jolla, CA) was used for all analyses. *p*-Values ≤ 0.05 were considered statistically significant.

RESULTS

Skewing of X-inactivation in explanted OTC-deficient pediatric liver tissue

Explanted pediatric livers were obtained at the time of orthotopic liver transplantation (OLT) from two unrelated female patients heterozygous for OTC deficiency (designated as OTC3 and OTC5) and an affected male sibling of OTC5 (designated as OTC2). Intact liver tissue was set aside, and the remaining tissue was dissociated for cryopreservation and subsequent engraftment into FRG mice.

Patients OTC3 and OTC2 presented with hyperammonemia, while patient OTC5 presented with both hyperammonemia and episodes of acute liver failure. The

mutation in the siblings, patients OTC5 and OTC2, has been described,¹³ but the putative disease-causing mutation in patient OTC3 has not been reported.

Differing levels of liver-wide OTC enzyme activity in samples of liver tissue from two female patients, OTC3 and OTC5, provided an initial indication of marked skewing of X-inactivation in patient OTC3 in favor of the X chromosome bearing the wild-type OTC allele (Table 1). As expected, the level of liver-wide OTC enzymatic activity in the male patient, OTC2, was low, consistent with the early need for OLT.

Analysis of OTC expression in fixed liver sections by immunohistochemistry (IHC) and *in situ* OTC activity staining confirmed the presence of marked skewing in patient OTC3, but minimal evidence of skewing in patient OTC5 (Fig. 1A, B). The levels of skewing were quantified by both IHC image analysis (Fig. 1C) and FACS of dissociated hepatocytes (Fig. 1D), with the different measures being in broad agreement.

Analysis of human OTC allelic mRNA expression by Sanger sequencing was supportive of skewing in both patients (Fig. 1E), but not conducive to quantitation given the inherent variability in amplitude of the signal for individual bases in the sequence trace.

Recapitulation of skewed X-inactivation in patient-derived hepatocytes following engraftment in the FRG mouse liver

Dissociated patient hepatocytes were used to create chimeric mouse–human livers by engraftment and expansion in the FRG mouse (hFRG) (Fig. 2A). Importantly, IHC analysis of hFRG liver sections revealed distinctly clonal clusters of either OTC-positive or OTC-negative human hepatocytes (Fig. 2B).

Numerical analysis of the relative numbers of OTC-positive and OTC-negative clonal clusters of human hepatocytes and FACS analysis of the human hepatocyte fraction in dissociated hFRG liver samples confirmed recapitulation of the skewing observed in native liver tissue from patient OTC3 and evidence of modest skewing in patient OTC5 (Fig. 2C, D). Analysis of human OTC allelic mRNA expression in hFRG liver tissue by Sanger sequencing again suggested skewing in both patients (Fig. 2E).

Table 1. Patient details, ornithine transcarbamylase mutation, and liver-wide enzymatic activity

Sex	Patient ID	Age at OLT	Disease-Causing Mutation	OTC Activity (% Wild-Type)
Female	OTC3	6 years	Missense, exon 5 c.407A > G (p.D136G)	6.9 \pm 1.0
Female	OTC5	22 months	Missense, exon 6 c.621C > A (p.S207R)	57.5 \pm 3.3
Male	OTC2	6 months	Missense, exon 6 c.621C > A (p.S207R)	3.8 \pm 0.8

OLT, orthotopic liver transplantation; OTC, ornithine transcarbamylase.

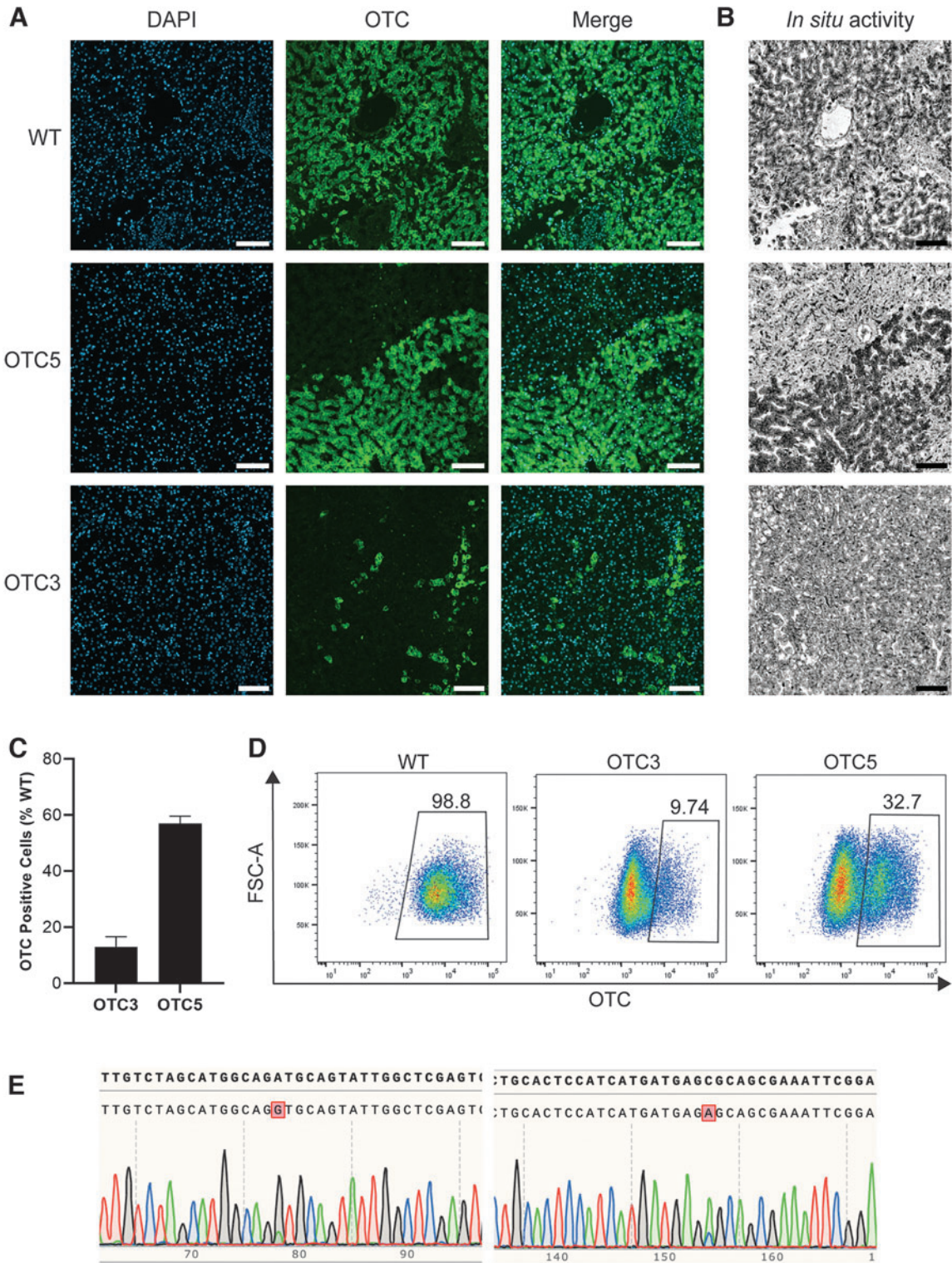


Figure 1. Direct evaluation of skewing in explanted patient liver. **(A)** Representative images showing OTC expression by IHC in WT and patient liver sections. Individual cells were identified by nuclear staining with DAPI (blue). Scale bar=500 μm . **(B)** Corresponding representative images showing OTC enzymatic activity *in situ* in WT and patient liver sections. Darker cells represent higher OTC activity. Scale bar=500 μm . **(C)** Estimation of the percentage of OTC-positive cells in patient liver sections (three composite sections per patient, $\sim 3 \times 10^7 \mu\text{m}^2$ per section) by IHC, based on quantitation of OTC-positive area. Error bars represent standard error of the mean. **(D)** Quantitation of OTC-positive hepatocytes in dissociated WT and patient liver samples by FACS. **(E)** Sanger sequencing chromatograms of OTC cDNA showing the mutant and WT peaks in patient OTC3 (left panel) and patient OTC5 (right panel). The upper sequence is the WT, and the lower sequence is the patient. The mutant base is boxed in red. DAPI, 4',6'-diamidino-2-phenylindole; FACS, fluorescence-activated cell sorting; FSC-A, forward scatter; *OTC3/OTC5*/IHC, immunohistochemistry; OTC, ornithine transcarbamylase; WT, wild-type.

The presence of distinct OTC-positive or OTC-negative human hepatocyte clusters offered further opportunity to assess the relative growth rate of the two populations by analysis of cluster size in fixed sections. No significant size difference was observed (data not shown).

Engraftment of patient hepatocytes induces a treatable biochemical phenotype

To explore the utility of the model system described for evaluation of therapeutic interventions, mice engrafted with hepatocytes derived from patient OTC3 were monitored for elevation of urinary orotate, a readily measurable biochemical marker of proximal urea cycle enzyme deficiencies (Fig. 3A).

Mice engrafted with patient-derived hepatocytes not only showed marked elevation of urinary orotate but also showed complete normalization of this biomarker when engrafted mice were treated using a conventional gene addition strategy with an AAV vector encoding human OTC pseudo-serotyped with the human liver tropic LK03 capsid⁸ (Fig. 3B).

Statistical analysis using two-way repeated-measures ANOVA confirmed statistically significant interactions between vector treatment ($p < 0.0001$) and orotate levels ($p < 0.01$), as well as a statistically significant interaction between sampling time and orotate levels within treatment groups ($p < 0.0001$; Supplementary Table S2).

DISCUSSION

Manipulation of the epigenome is evolving as a promising therapeutic approach in the treatment of an array of disorders ranging from those with relatively simple Mendelian inheritance to those with complex multifactorial disease states with both genetic and environmental components.¹⁴ This is becoming increasingly feasible with growing understanding of the mechanisms involved in epigenetic gene regulation and the availability of tools for epigenetic manipulation and assays to assess the resultant effects.

In the context of therapeutic application, a major remaining challenge, however, is the availability of pre-clinical model systems that not only recapitulate disease pathophysiology but are also clinically predictive.

We and others have used the FRG mouse model to develop novel AAV capsid technology for enhanced gene delivery to the human liver^{8,12,15–23} and explore novel therapeutic interventions involving gene addition and genome editing technology.²⁴ In this study, we show that this powerful model system can also be configured to explore therapeutic manipulation of the epigenome.

Access to explanted disease-affected female livers has allowed exploration of the possibility of reactivating silenced wild-type alleles on the inactive X chromosome, in the context of heterozygous OTC deficiency in symptomatic female patients. Skewing of inactivation in favor of the X chromosome carrying the wild-type allele is commonly associated with increased disease severity.

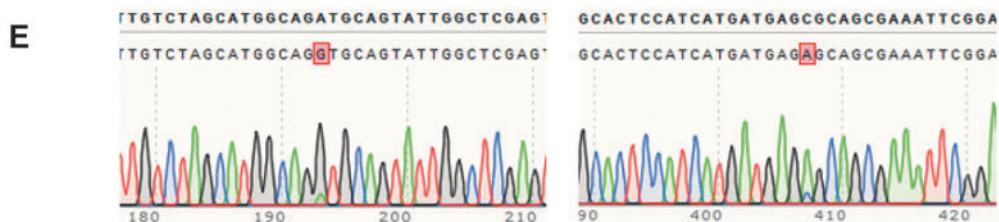
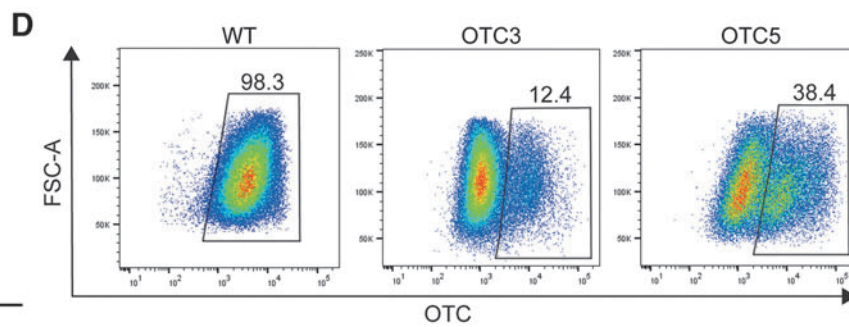
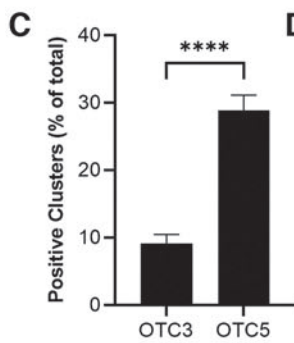
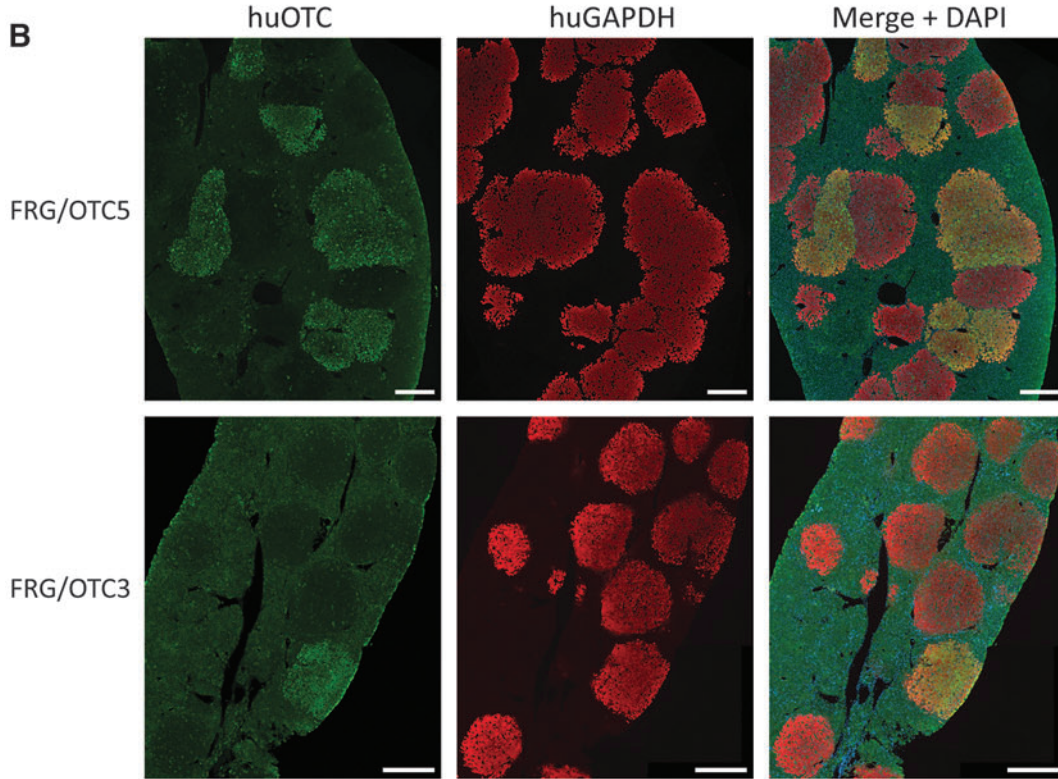
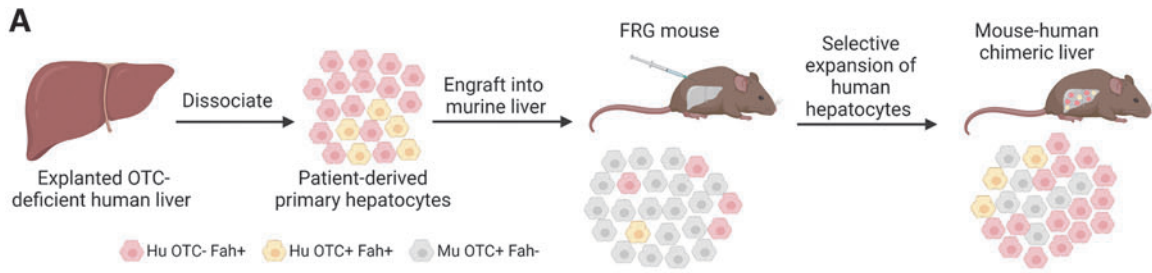
Dissociated patient hepatocytes were successfully deployed in the FRG mouse to establish chimeric mouse–human livers.⁷ Critically, the resultant discrete clusters of human hepatocytes proved to be either OTC positive or negative, consistent with clonal expansion from individual hepatocytes in which either the X chromosome carrying the mutant or wild-type allele was inactivated, respectively.

Even more germane was the observation that within the limits of sampling error, the proportions of OTC-positive and -negative clonal clusters of human hepatocytes recapitulated the levels of skewing in the native explanted liver tissue from which the hepatocytes were initially recovered. An incidental observation of relevance to disease pathophysiology in affected female patients was the equivalent mean size of OTC-positive and -negative human hepatocyte clusters.

This implies that at least in the context of the chimeric mouse–human liver, there is no differential growth advantage between the OTC-positive and -negative hepatocyte populations, which aligns with the lack of published evidence for changes in disease phenotype over time in individual symptomatic heterozygous females.

Importantly, engraftment and expansion of OTC-deficient human hepatocytes in the FRG mouse liver resulted in a readily measurable metabolic phenotype, the appearance of orotate in host mouse urine. Moreover, the utility of orotate as a biomarker for the efficacy of therapeutic interventions aimed at restoring OTC enzymatic activity in deficient human hepatocytes was confirmed by

Figure 2. Recapitulation of skewed X-inactivation in the FRG mouse. **(A)** Schematic diagram showing establishment of chimeric mouse–human livers following engraftment of human hepatocytes from dissociated patient liver explants. **(B)** Representative images of liver sections from recipient FRG mice engrafted with hepatocytes from patient OTC5 (FRG/OTC5) and patient OTC3 (FRG/OTC3) showing colocalization of huGAPDH (red) and huOTC (green) by IHC. The human OTC-positive hepatocytes are visualized as orange in the overlay. Individual cells were identified by nuclear staining with DAPI (blue). Scale bar = 500 μ m. **(C)** Percentage of OTC-positive human hepatocyte clonal clusters. FRG/OTC3, six mice; FRG/OTC5, three mice; four composite liver sections analyzed per mouse ($\sim 3 \times 10^7 \mu\text{m}^2$ per section). Error bars represent standard error of the mean. For statistical comparison, the nonparametric Mann–Whitney *U* test was used (**** $p < 0.0001$). **(D)** Quantitation of OTC-positive human hepatocytes isolated from dissociated chimeric FRG liver by FACS. **(E)** Sanger sequencing chromatograms of OTC cDNA showing mutant and WT peaks in dissociated human hepatocytes isolated from mice engrafted with cells from patient OTC3 (left panel) and patient OTC5 (right panel). The upper sequence is the WT, and the lower sequence is the patient. The mutant base is boxed in red. Fah+, fumarylacetoacetase positive; FRG, Fah^{-/-}/Rag2^{-/-}/IL2rg^{-/-} mouse model; GAPDH, glyceraldehyde 3-phosphate dehydrogenase; Hu, human; huGAPDH, human hepatocytes expressing GAPDH; huOTC, human hepatocytes expressing OTC; OTC-, OTC negative, OTC+, OTC positive.



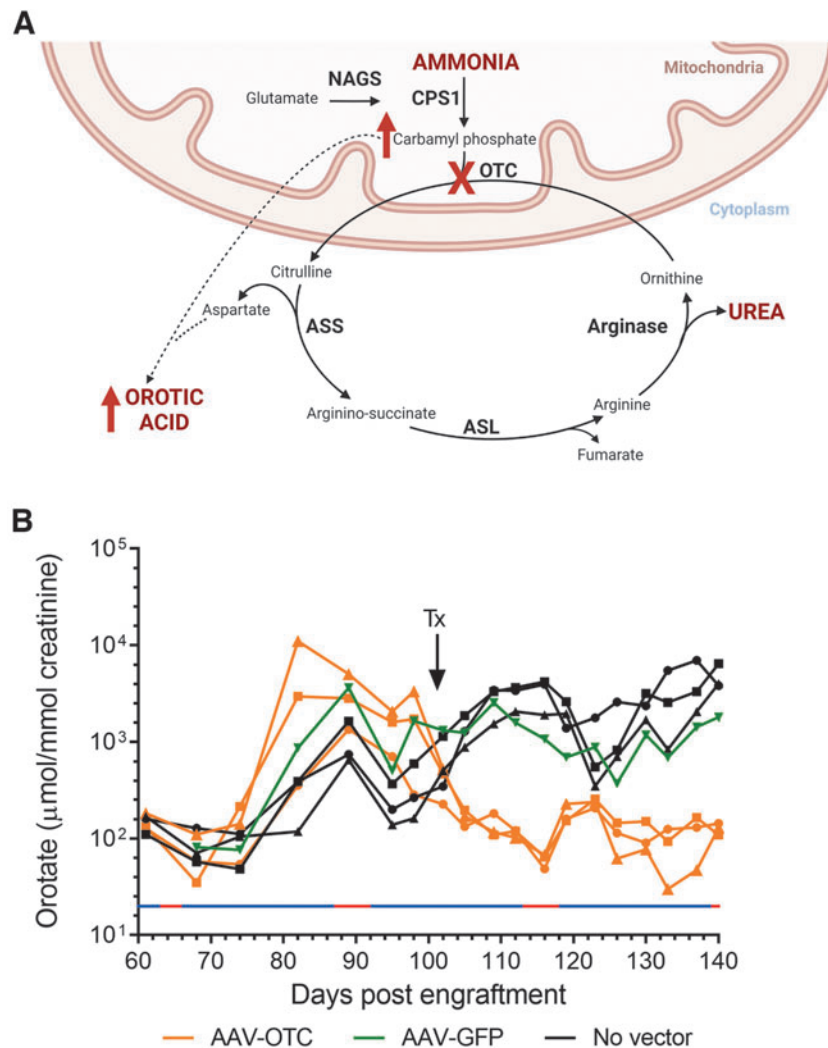


Figure 3. Induction of a readily measurable biochemical phenotype in FRG mice. **(A)** Diagram of the urea cycle showing increased orotate production accompanying deficiencies in OTC enzymatic activity due to accumulation of carbamyl phosphate. **(B)** Orotate levels (normalized to creatinine) in the urine of FRG mice engrafted with OTC3 patient cells, pre- and post-treatment (Tx) with a conventional AAV vector (pseudo-serotyped with the LK03 capsid) encoding a human codon-optimized OTC (AAV-OTC). The vector dose was 5×10^{11} vector genomes per mouse. Controls include mice either untreated (no vector) or injected with a vector encoding GFP (AAV-GFP). Drinking water cycling conditions are indicated (blue line, without NTBC; red line, with NTBC). Two-way repeated-measures ANOVA was used to calculate the significance between treatment groups over time (Supplementary Table S2). AAV, adeno-associated virus; ANOVA, analysis of variance; GFP, enhanced green fluorescent protein; NTBC, 2-(2-nitro-4-trifluoromethylbenzoyl)-1,3-cyclohexanedione.

normalization of orotate levels following systemic delivery of a conventional gene addition AAV vector.

Thus, the model system not only recapitulates skewing of X chromosome inactivation but it can also be configured to evaluate *in vivo* interventions that reconstitute OTC activity in deficient human hepatocytes, including reactivation of silenced wild-type OTC alleles by manipulation of the epigenome.

Toward this end, current liver-targeted gene transfer technologies, including AAV vectors and lipid nanoparticles, can be readily repurposed to deliver epigenetic effectors with high efficiency.^{25–28} These effectors can be delivered alone or in combination to alter DNA methylation, modify chromatin, or drive transactivation at precise genomic loci.²⁹

While the model system described has many positive attributes, it is logistically challenging. The leading limitation is acquisition of explanted diseased human livers and the need to cryopreserve sufficient dissociated hepatocytes for completion of potentially demanding studies. One possible strategy to partially mitigate this challenge is to expand human hepatocytes in primary recipient mice and undertake studies in secondary recipients.

We and others⁷ have successfully used this approach with healthy donor hepatocytes, but are yet to undertake comprehensive studies in patient-derived hepatocytes required to confirm maintenance of X-inactivation in concert with serial passaging, which involves supraphysiological levels of hepatocellular replication.

In summary, we report a novel *in vivo* model system that faithfully recapitulates skewing of X chromosome inactivation in female patient-derived primary human hepatocytes. While our primary intent is to use this system to explore locus-specific therapeutic reactivation of wild-type OTC alleles on inactivated X chromosomes, it should prove equally powerful for more basic studies exploring epigenetic mechanisms involved in maintenance of repression and derepression of gene expression.

Moreover, the system reported has the potential to offer broader insights into the many conditions with major epigenetic influences.³⁰

ACKNOWLEDGMENTS

The authors thank Li Ma at The Westmead Institute for Medical Research for embedding and sectioning tissue; Leszek Lisowski for providing the LK03 capsid plasmid; and the patients and their families.

AUTHORS' CONTRIBUTIONS

I.E.A. and S.C.C. were involved in concept and design of the study, writing of the article, analysis, and interpretation of data. S.C.C., E.B.v.D., M.S., M.M., and E.Z. were

involved in development of methodology and execution of experiments, analysis and interpretation of data, and preparation of figures. S.S. and K.B. were involved with attending physicians and hospital liaison with respect to obtaining patient liver explants. B.D. and A.A.T. were involved in technical support and analysis and interpretation of data with regard to biochemical analyses. A.K., L.W., and N.A. provided bioinformatic assistance. P.G. and J.B. were collaborators involved in the design of the AAV vector studies. All authors read and approved the final article.

AUTHOR DISCLOSURE

No competing financial interests exist.

FUNDING INFORMATION

This study was, in part, supported by funding from Luminesce Alliance (LA016).

SUPPLEMENTARY MATERIAL

Supplementary Table S1
Supplementary Table S2

REFERENCES

- Lyon MF. Gene action in the X-chromosome of the Mouse (*Mus musculus* L.). *Nature* 1961; 190(4773):372–373.
- Migeon BR. X-linked diseases: Susceptible females. *Genet Med* 2020;22(7):1156–1174.
- Carrette LLG, Wang CY, Wei C, et al. A mixed modality approach towards Xi reactivation for Rett syndrome and other X-linked disorders. *Proc Natl Acad Sci* 2018;115(4):E668–E675.
- Liu XS, Wu H, Krzisch M, et al. Rescue of fragile X syndrome neurons by DNA methylation editing of the FMR1 gene. *Cell* 2018;172(5):979.e6–992.e6.
- Halmai JANM, Deng P, Gonzalez CE, et al. Artificial escape from XCI by DNA methylation editing of the CDKL5 gene. *Nucleic Acids Res* 2020;48(5): 2372–2387.
- Summar ML, Dobbelaere D, Brusilow S, et al. Diagnosis, symptoms, frequency and mortality of 260 patients with urea cycle disorders from a 21-year, multicentre study of acute hyperammonaemic episodes. *Acta Paediatr Oslo Nor* 1992 2008;97(10):1420–1425.
- Azuma H, Paulk N, Ranade A, et al. Robust expansion of human hepatocytes in *Fah^{-/-}/Rag2^{-/-}/Il2rg^{-/-}* mice. *Nat Biotechnol* 2007;25(8):903–910.
- Lisowski L, Dane AP, Chu K, et al. Selection and evaluation of clinically relevant AAV variants in a xenograft liver model. *Nature* 2014;506(7488): 382–386.
- Lee SML, Schelcher C, Demmel M, et al. Isolation of human hepatocytes by a two-step collagenase perfusion procedure. *J Vis Exp* 2013;(79):50615.
- Ye X, Robinson MB, Batshaw ML, et al. Prolonged metabolic correction in adult ornithine transcarbamylase-deficient mice with adenoviral vectors. *J Biol Chem* 1996;271(7):3639–3646.
- Schindelin J, Arganda-Carreras I, Frise E, et al. Fiji: An open-source platform for biological-image analysis. *Nat Methods* 2012;9(7):676–682.
- Cabanes-Creus M, Hallwirth CV, Westhaus A, et al. Restoring the natural tropism of AAV2 vectors for human liver. *Sci Transl Med* 2020; 12(560):eaba3312.
- Shimadzu M, Matsumoto H, Matsuura T, et al. Ten novel mutations of the ornithine transcarbamylase (OTC) gene in OTC deficiency. *Hum Mutat* 1998;Suppl. 1:S5–S7.
- Nakamura M, Gao Y, Dominguez AA, et al. CRISPR technologies for precise epigenome editing. *Nat Cell Biol* 2021;23(1):11–22.
- Pei X, Shao W, Xing A, et al. Development of AAV variants with human hepatocyte tropism and neutralizing antibody escape capacity. *Mol Ther Methods Clin Dev* 2020;18:259–268.
- Westhaus A, Cabanes-Creus M, Jonker T, et al. AAV-p40 bioengineering platform for variant selection based on transgene expression. *Hum Gene Ther* 2022;33(11–12):664–682.
- Westhaus A, Cabanes-Creus M, Rybicki A, et al. High-throughput *in vitro*, *ex vivo*, and *in vivo* screen of adeno-associated virus vectors based on physical and functional transduction. *Hum Gene Ther* 2020;31(9–10):575–589.
- Cabanes-Creus M, Navarro RG, Zhu E, et al. Novel human liver-tropic AAV variants define transferable domains that markedly enhance the human tropism of AAV7 and AAV8. *Mol Ther Methods Clin Dev* 2022;24:88–101.
- Paulk NK, Pekrun K, Zhu E, et al. Bioengineered AAV capsids with combined high human liver transduction *in vivo* and unique humoral seroreactivity. *Mol Ther* 2018;26(1):289–303.
- Shao W, Pei X, Cui C, et al. Superior human hepatocyte transduction with adeno-associated virus vector serotype 7. *Gene Ther* 2019;26(12):504–514.

21. Cabanes-Creus M, Ginn SL, Amaya AK, et al. Codon-optimization of wild-type adeno-associated virus capsid sequences enhances DNA family shuffling while conserving functionality. *Mol Ther Methods Clin Dev* 2019;12:71–84.
22. Cabanes-Creus M, Westhaus A, Navarro RG, et al. Attenuation of heparan sulfate proteoglycan binding enhances in vivo transduction of human primary hepatocytes with AAV2. *Mol Ther Methods Clin Dev* 2020;17:1139–1154.
23. Meumann N, Cabanes-Creus M, Ertelt M, et al. Adeno-associated virus serotype 2 capsid variants for improved liver-directed gene therapy. *Hepatology* (Baltimore, MD) 2023;77(3):802–815.
24. Ginn SL, Amaya AK, Liao SHY, et al. Efficient in vivo editing of OTC-deficient patient-derived primary human hepatocytes. *JHEP Rep Innov Hepatol* 2020;2(1):100065.
25. Hunt C, Hartford SA, White D, et al. Tissue-specific activation of gene expression by the Synergistic Activation Mediator (SAM) CRISPRa system in mice. *Nat Commun* 2021;12(1):2770.
26. Beyersdorf JP, Bawage S, Iglesias N, et al. Robust, durable gene activation in vivo via mRNA-encoded activators. *ACS Nano* 2022;16(4):5660–5671.
27. Lau CH, Suh Y. In vivo epigenome editing and transcriptional modulation using CRISPR technology. *Transgenic Res* 2018;27(6):489–509.
28. Yamamoto N, Morita S, Hatada I, et al. Engineering of AAV-mediated in vivo targeted DNA methylation editing system via staphylococcus aureus derived Cas9-SunTag [internet]. In review; 2021. Available from: <https://www.researchsquare.com/article/rs-1065603/v1> [Last accessed: December 19, 2022].
29. Holtzman L, Gersbach CA. Editing the epigenome: Reshaping the genomic landscape. *Annu Rev Genomics Hum Genet* 2018;19(1):43–71.
30. Portela A, Esteller M. Epigenetic modifications and human disease. *Nat Biotechnol* 2010;28(10):1057–1068.

Received for publication January 22, 2023;
accepted after revision May 31, 2023.

Published online: June 22, 2023.